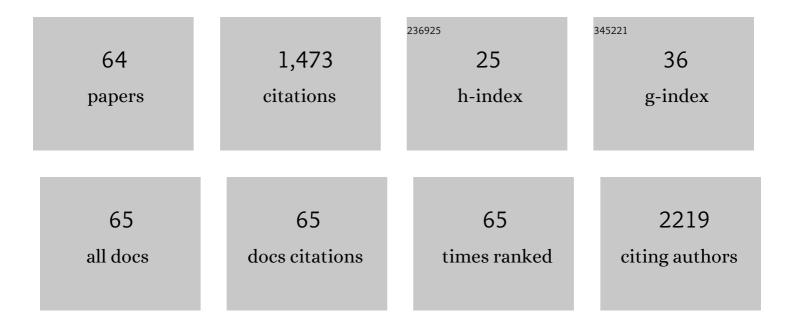
List of Publications by Year in descending order

Source: https://exaly.com/author-pdf/1970230/publications.pdf Version: 2024-02-01



#	Article	IF	CITATIONS
1	SEDS–bPBP pairs direct lateral and septal peptidoglycan synthesis in Staphylococcus aureus. Nature Microbiology, 2019, 4, 1368-1377.	13.3	77
2	Mixing Block Copolymers with Phospholipids at the Nanoscale: From Hybrid Polymer/Lipid Wormlike Micelles to Vesicles Presenting Lipid Nanodomains. Langmuir, 2017, 33, 1705-1715.	3.5	75
3	Phase Separation and Nanodomain Formation in Hybrid Polymer/Lipid Vesicles. ACS Macro Letters, 2015, 4, 182-186.	4.8	69
4	Role of Helix 0 of the N-BAR Domain in Membrane Curvature Generation. Biophysical Journal, 2008, 94, 3065-3073.	0.5	58
5	Effects of fluorescent probe NBD-PC on the structure, dynamics and phase transition of DPPC. A molecular dynamics and differential scanning calorimetry study. Biochimica Et Biophysica Acta - Biomembranes, 2008, 1778, 491-501.	2.6	58
6	Modulation of phase separation at the micron scale and nanoscale in giant polymer/lipid hybrid unilamellar vesicles (GHUVs). Soft Matter, 2017, 13, 627-637.	2.7	57
7	Pdr18 is involved in yeast response to acetic acid stress counteracting the decrease of plasma membrane ergosterol content and order. Scientific Reports, 2018, 8, 7860.	3.3	54
8	Ca2+ induces PI(4,5)P2 clusters on lipid bilayers at physiological PI(4,5)P2 and Ca2+ concentrations. Biochimica Et Biophysica Acta - Biomembranes, 2014, 1838, 822-830.	2.6	47
9	Comparative Transcriptomic Analysis of the Burkholderia cepacia Tyrosine Kinase bceF Mutant Reveals a Role in Tolerance to Stress, Biofilm Formation, and Virulence. Applied and Environmental Microbiology, 2013, 79, 3009-3020.	3.1	45
10	Dependence of M13 Major Coat Protein Oligomerization and Lateral Segregation on Bilayer Composition. Biophysical Journal, 2003, 85, 2430-2441.	0.5	42
11	Quantification of Protein-Lipid Selectivity using FRET: Application to the M13 Major Coat Protein. Biophysical Journal, 2004, 87, 344-352.	0.5	42
12	Quantification of protein–lipid selectivity using FRET. European Biophysics Journal, 2010, 39, 565-578.	2.2	40
13	Reorganization of lipid domain distribution in giant unilamellar vesicles upon immobilization with different membrane tethers. Biochimica Et Biophysica Acta - Biomembranes, 2012, 1818, 2605-2615.	2.6	38
14	A combined fluorescence spectroscopy, confocal and 2-photon microscopy approach to re-evaluate the properties of sphingolipid domains. Biochimica Et Biophysica Acta - Biomembranes, 2013, 1828, 2099-2110.	2.6	38
15	Membrane properties of giant polymer and lipid vesicles obtained by electroformation and pva gel-assisted hydration methods. Colloids and Surfaces A: Physicochemical and Engineering Aspects, 2017, 533, 347-353.	4.7	38
16	Absence of clustering of phosphatidylinositol-(4,5)-bisphosphate in fluid phosphatidylcholine. Journal of Lipid Research, 2006, 47, 1521-1525.	4.2	37
17	Cytotoxic bile acids, but not cytoprotective species, inhibit the ordering effect of cholesterol in model membranes at physiologically active concentrations. Biochimica Et Biophysica Acta - Biomembranes, 2013, 1828, 2152-2163.	2.6	36
18	Deoxycholic acid modulates cell death signaling through changes in mitochondrial membrane properties. Journal of Lipid Research, 2015, 56, 2158-2171.	4.2	36

#	Article	IF	CITATIONS
19	Biophysical study of human induced Pluripotent Stem Cell-Derived cardiomyocyte structural maturation during long-term culture. Biochemical and Biophysical Research Communications, 2018, 499, 611-617.	2.1	35
20	Ciprofloxacin interactions with bacterial protein OmpF: Modelling of FRET from a multi-tryptophan protein trimer. Biochimica Et Biophysica Acta - Biomembranes, 2007, 1768, 2822-2830.	2.6	33
21	Membrane microheterogeneity: Förster resonance energy transfer characterization of lateral membrane domains. European Biophysics Journal, 2010, 39, 589-607.	2.2	33
22	Modulation of membrane properties of lung cancer cells by azurin enhances the sensitivity to EGFR-targeted therapy and decreased β1 integrin-mediated adhesion. Cell Cycle, 2016, 15, 1415-1424.	2.6	33
23	High performance NIR fluorescent silica nanoparticles for bioimaging. RSC Advances, 2013, 3, 9171.	3.6	29
24	NIR and visible perylenediimide-silica nanoparticles for laser scanning bioimaging. Dyes and Pigments, 2014, 110, 227-234.	3.7	28
25	Characterization of a Squaraine/Chitosan System for Photodynamic Therapy of Cancer. Journal of Physical Chemistry B, 2016, 120, 1212-1220.	2.6	27
26	Yeast adaptive response to acetic acid stress involves structural alterations and increased stiffness of the cell wall. Scientific Reports, 2021, 11, 12652.	3.3	25
27	Azurin interaction with the lipid raft components ganglioside GM-1 and caveolin-1 increases membrane fluidity and sensitivity to anti-cancer drugs. Cell Cycle, 2018, 17, 1649-1666.	2.6	24
28	Improved Parameterization of Phosphatidylinositide Lipid Headgroups for the Martini 3 Coarse-Grain Force Field. Journal of Chemical Theory and Computation, 2022, 18, 357-373.	5.3	24
29	The mechanism of action of pepR, a viral-derived peptide, against Staphylococcus aureus biofilms. Journal of Antimicrobial Chemotherapy, 2019, 74, 2617-2625.	3.0	23
30	Silica nanoparticles with thermally activated delayed fluorescence for live cell imaging. Materials Science and Engineering C, 2020, 109, 110528.	7.3	23
31	Characterization of BCAM0224, a Multifunctional Trimeric Autotransporter from the Human Pathogen Burkholderia cenocepacia. Journal of Bacteriology, 2014, 196, 1968-1979.	2.2	20
32	The combination of block copolymers and phospholipids to form giant hybrid unilamellar vesicles (GHUVs) does not systematically lead to "intermediate―membrane properties. Soft Matter, 2018, 14, 6476-6484.	2.7	20
33	Intrinsically Fluorescent Silica Nanocontainers: A Promising Theranostic Platform. Microscopy and Microanalysis, 2013, 19, 1216-1221.	0.4	19
34	The Tyrosine Kinase BceF and the Phosphotyrosine Phosphatase BceD of Burkholderia contaminans Are Required for Efficient Invasion and Epithelial Disruption of a Cystic Fibrosis Lung Epithelial Cell Line. Infection and Immunity, 2015, 83, 812-821.	2.2	18
35	<i>Staphylococcus aureus</i> haem biosynthesis and acquisition pathways are linked through haem monooxygenase IsdG. Molecular Microbiology, 2018, 109, 385-400.	2.5	18
36	Role of calcium in membrane interactions by PI(4,5)P2-binding proteins. Biochemical Society Transactions, 2014, 42, 1441-1446.	3.4	16

#	Article	IF	CITATIONS
37	Crosstalk between Yeast Cell Plasma Membrane Ergosterol Content and Cell Wall Stiffness under Acetic Acid Stress Involving Pdr18. Journal of Fungi (Basel, Switzerland), 2022, 8, 103.	3.5	15
38	Binding assays of inhibitors towards selected V-ATPase domains. Biochimica Et Biophysica Acta - Biomembranes, 2006, 1758, 1777-1786.	2.6	13
39	Electrostatically driven lipid–protein interaction: Answers from FRET. Biochimica Et Biophysica Acta - Biomembranes, 2015, 1848, 1837-1848.	2.6	13
40	Membrane Order Is a Key Regulator of Divalent Cation-Induced Clustering of PI(3,5)P <sub>2</sub> and PI(4,5)P <sub>2</sub> . Langmuir, 2017, 33, 12463-12477.	3.5	13
41	Structure and Lateral Organization of Phosphatidylinositol 4,5-bisphosphate. Molecules, 2020, 25, 3885.	3.8	13
42	Quantitative Evaluation of DNA Dissociation from Liposome Carriers and DNA Escape from Endosomes During Lipid-Mediated Gene Delivery. Human Gene Therapy Methods, 2014, 25, 303-313.	2.1	10
43	A Case of Selfâ€Organization in Highly Emissive Eu <sup>III</sup> Ionic Liquids. European Journal of Inorganic Chemistry, 2017, 2017, 3429-3434.	2.0	10
44	Engineering Boron Hot Spots for the Siteâ€selective Installation of Iminoboronates on Peptide Chains. Chemistry - A European Journal, 2020, 26, 15226-15231.	3.3	8
45	Electrostatically driven lipid–lysozyme mixed fibers display a multilamellar structure without amyloid features. Soft Matter, 2014, 10, 840-850.	2.7	7
46	The Azurin-Derived Peptide CT-p19LC Exhibits Membrane-Active Properties and Induces Cancer Cell Death. Biomedicines, 2021, 9, 1194.	3.2	6
47	Interaction of the Indole Class of Vacuolar H+-ATPase Inhibitors with Lipid Bilayersâ€. Biochemistry, 2006, 45, 5271-5279.	2.5	5
48	Accurate quantification of inter-domain partition coefficients in GUVs exhibiting lipid phase coexistence. RSC Advances, 2016, 6, 66641-66649.	3.6	5
49	Disclosing azole resistance mechanisms in resistant <i>Candida glabrata</i> strains encoding wild-type or gain-of-function <i>CgPDR1</i> alleles through comparative genomics and transcriptomics. G3: Genes, Genomes, Genetics, 2022, 12, .	1.8	5
50	Acyl-chain saturation regulates the order of phosphatidylinositol 4,5-bisphosphate nanodomains. Communications Chemistry, 2021, 4, .	4.5	4
51	The BASHY Platform Enables the Assembly of a Fluorescent Bortezomib–GV1001 Conjugate. ACS Medicinal Chemistry Letters, 2022, 13, 128-133.	2.8	4
52	New Visible and NIR Highly Photostable Fluorescent Silica Nanoparticles for Laser Scanning Imaging Applications. Microscopy and Microanalysis, 2013, 19, 105-106.	0.4	2
53	The Cytotoxic Bile Acid DCA Modulates Apoptotic Signalling through Alteration of Mitochondrial Membrane Properties. Biophysical Journal, 2015, 108, 242a.	0.5	1
54	Förster Resonance Energy Transfer as a Tool for Quantification of Protein–Lipid Selectivity. Methods in Molecular Biology, 2019, 2003, 369-382.	0.9	1

#	Article	IF	CITATIONS
55	Measuring the Impact of Bile Acids on the Membrane Order of Primary Hepatocytes and Isolated Mitochondria by Fluorescence Imaging and Spectroscopy. Methods in Molecular Biology, 2019, 1981, 99-115.	0.9	1
56	Advanced FRET Methodologies: Protein–Lipid Selectivity Detection and Quantification. Advances in Experimental Medicine and Biology, 2012, 749, 171-185.	1.6	1
57	Quantitative FRET Microscopy Reveals a Crucial Role of Cytoskeleton in Promoting PI(4,5)P2 Confinement. International Journal of Molecular Sciences, 2021, 22, 11727.	4.1	1
58	Quantitative Analysis of Domain Formation after Snare Mediated Fusion of Synaptic Vesicles. Biophysical Journal, 2010, 98, 678a.	0.5	0
59	High Affinity Immobilization of Giant Unilamellar Vesicles (GUVs) Induces Redistribution of Lipid Domains. Biophysical Journal, 2012, 102, 295a.	0.5	0
60	The Apoptotic Bile Acid DCA has Preference for Association to Liquid Disordered Lipid Domains and Inhibits the Rigidifying Effect of Cholesterol in Membranes. Biophysical Journal, 2013, 104, 586a.	0.5	0
61	Physiological Calcium Concentrations Induce PI(4,5)P2 Clustering: PI(4,5)P2 as a Lipidic Calcium Sensor. Biophysical Journal, 2013, 104, 372a.	0.5	0
62	Förster Resonance Energy Transfer as a Tool for Quantification of Protein–Lipid Selectivity. Methods in Molecular Biology, 2013, 974, 219-232.	0.9	0
63	P116 INTERACTION OF APOPTOTIC AND CYTOPROTECTIVE BILE ACIDS WITH BIOMEMBRANES. Journal of Hepatology, 2014, 60, S105.	3.7	0
64	Impact of Ca2+-Induced PI(4,5)P2 Clusters on PH-YFP Organization and Protein-Protein Interactions. Biomolecules, 2022, 12, 912.	4.0	0